Predicting Fracture from Thermodynamic Modeling of Cementitious Systems

by Y. Wang, K. Bharadwaj, H. S. Esmaeeli, P. Zavattieri, O. B. Isgor, and W. J. Weiss

This paper describes an approach to predict the mechanical and fracture behavior of cement-based systems by combining thermodynamic and finite element analysis models. First, the reaction products in a hydrated cementitious paste are predicted using a thermodynamic model. Second, a pore partitioning model is used to segment the total porosity into porosity associated with gel pores and capillary pores. A property-porosity relationship is used to predict the elastic modulus, tensile strength, and fracture energy of the hardened cement paste. The paste's modulus, fracture energy, and tensile strength, along with information on the aggregate properties and interfacial transition zone properties, are used as inputs to a finite element analysis model to predict the flexural strength and fracture response of mortars.

Keywords: elastic modulus; finite element analysis (FEA); fracture; mechanics; porosity; tensile strength; thermodynamic modeling.

INTRODUCTION

The concrete industry is actively working on reducing the CO_2 emissions associated with conventional concrete manufacture through several approaches.[1,2] First, the clinker content of concrete can be reduced by substituting a portion of the ordinary portland cement (OPC) with supplementary cementitious materials (SCM) or filler powders.[3-7] Second, the paste content in the concrete can be reduced through appropriate mixture design.[8-11] Third, the service life of the concrete can be improved, thereby reducing the annual carbon content.

This paper discusses an approach to lower the cement content used in concrete through improved mixture design by providing a tool to predict the mechanical behavior of concrete more accurately. Conventional mixture design approaches often rely on the use of empirical/experimental predictions of the performance of concrete,[12] especially when nonconventional cements and SCMs like fly ash, slag, silica fume, and so on, are used.[13] This often does not take full advantage of the benefits of the SCM being added to the system, such as improvements to the compressive strength of concrete made with the SCM.[14-17] Sometimes, empirical modifications are made to predict the compressive strength of systems containing SCMs like fly ash[18]; however, these calibrations are typically SCM-specific. Many historical SCM sources are changing or becoming less available,[3,5,19] and as a result, there has been a desire to identify alternative SCMs (for example, municipal waste incineration ash, bottom ash, boiler slag, natural pozzolans, and agricultural waste ash),[20-29] and to develop approaches to use off-spec

materials.[20] Testing each SCM individually to predict the performance of concrete made with the SCM is time-consuming and expensive. There exists a need for robust tools to predict the performance of concrete using these SCMs (for example, strength, diffusivity, time to corrosion, shrinkage, and freezing-and-thawing performance).

There is a growing body of research that uses thermodynamic models to predict the reaction products for cementitious materials.[30-37] While powerful, these techniques do not describe the spatial distribution of these reaction products. For example, they can predict the total pore volume but not the size and distribution of the pores. To overcome this limitation, the authors have developed an approach, the pore partitioning model (PPM), to interpret the results of the thermodynamic calculations to predict the pore structure.[38,39] Computational tools have also been developed that can link thermodynamics, kinetics, pore structure information, and predicted performance.[17,40,41] This tool requires several inputs, including the chemistry of the binder used (OPC and SCM chemistries and contents, and the SCM reactivity, which can be measured using a pozzolanic reactivity test[42-44]), the physical properties of the concrete constituents (specific gravity and fineness of the OPC and SCMs, aggregate properties, and so on), and the mixture proportions of the concrete (amounts of air, paste, and aggregate). The tool can then be used for any cementitious material combination, in any proportion, to predict key properties of the hydrated system, including strength, porosity, electrical resistivity, formation factor, and ionic diffusion coefficients.[8,16,17,40,41] These predicted properties have been used to develop performance-based mixture proportioning methods[8,20] and service life prediction models.[45]

Despite these recent developments, there are opportunities to improve the models. For example, in the performance-based mixture design tool noted earlier,[8,20] the compressive strength was predicted using the empirical gel-space ratio from Powers and Brownyard,[46] which was developed for OPC systems. The flexural strength was then calculated using the empirical relation to compressive strength from ACI 318-19. Several researchers have been examining ways to improve the strength predictions for OPC + SCM systems,

such as coupling micromechanical models with thermodynamic modeling[15,47-51] or by using computer simulations such as CEMHYD3D.[52] Approaches using fractal scaling have also been proposed to predict the mechanical response of cementitious composites.[53] While these approaches are promising, there is a potential to predict mechanical behavior using fracture mechanics.[54-58] Fracture mechanics can natively predict flexural strength,[54,55,58] which can be used as a target criterion in the performance-based mixture design approach.

This paper proposes a framework that enables the mechanical and fracture behavior of a heterogenous concrete to be predicted using the chemical composition and reactivity of the cementitious materials used and the mixture proportions of the concrete. This is achieved through a four-step approach that predicts the reaction products of the paste and uses these products to determine the pore structure and mechanical properties. The framework is compared with experimental data on pastes and mortars. This framework is designed to be a generic tool that can be used to predict the fracture behavior of concrete using a wide variety of cement and alternative cement chemistries.

RESEARCH SIGNIFICANCE
This paper demonstrates a four-step framework to predict the mechanical response of cementitious composites using the outputs of thermodynamic modeling. Thermodynamic modeling is used to predict the reaction products, and a PPM predicts the porosity and pore volumes. This is used to predict the mechanical properties of the paste using property-porosity relationships and scaled to mortar and concrete using a finite element model (FEM). This approach considers the binder chemistry and pore volumes to predict concrete's mechanical properties. The FEM approach considers the natural variability in the cementitious matrix and aggregate shape and distribution.

MODELING FRAMEWORK
The modeling framework developed to predict the mechanical and fracture characteristics of cement paste and mortar in this paper consists of four parts and is shown in Fig. 1. First, the chemical composition of the cementitious binder and mass fraction of the constituents are combined with a thermodynamic modeling framework (that includes kinetics) to predict the reaction products of OPC and OPC + SCM pastes.[32-34,59,60] Next, the PPM is used to predict the paste porosity and volumes of different sizes of pores (gel and capillary pores).[38,39] The predicted pore volumes are then used as inputs to a property-porosity model[61,62] to predict the elastic modulus (E_p) and fracture energy (G_p^c) of the paste. The E_p and G_p^c are used to calculate the tensile strength of the paste (f_{tp}') using the concepts of linear-elastic fracture mechanics (LEFM). The E_p, G_p^c, and f_{tp}' are then used as inputs to an FEM to predict the mechanical and fracture behavior of mortar.

Thermodynamic model
Thermodynamic calculations are used to predict the volumes and compositions of the reaction products that form when cement paste hydrates. In this work, the GEMS3K software[63] is used in conjunction with the default PSI/Nagra database and the CemData v18.01 database[32] to predict the reaction products that form. This approach has been extensively validated and shown to accurately predict the reaction products of OPC and OPC + SCM systems.[32-34,63-65] While all possible phases that can form in cementitious binder systems are available in this database, the formation of siliceous hydrogarnet, carbonate-ettringite, and OH-hydrotalcite are blocked from forming based on evidence from the literature that these phases are unlikely to form in significant quantities at the time frames chosen in this study.[38,40] The H/S of the C-S-H formed in the simulations was also corrected based on recent experimental evidence.[32,65]

Thermodynamic modeling allows for calculating the products of the cementitious and pozzolanic reactions at thermodynamic equilibrium (that is, at an infinite time). However,
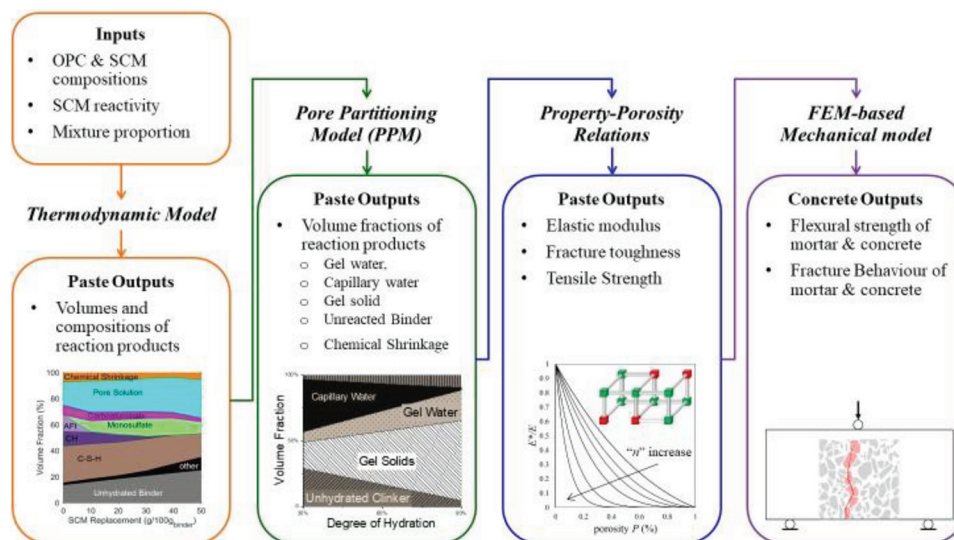
Fig. 1—Four-step modeling framework proposed consists of: (a) thermodynamic model; (b) pore partitioning model (PPM); (c) property-porosity relations; and (d) finite element model.

most cementitious systems are studied at a finite time and have not yet reached thermodynamic equilibrium. Kinetic models are often used in conjunction with thermodynamic models to predict the results of thermodynamic models at a given time. In this work, the modified Parrot-Killoh model[66] is used to calculate the degree of hydration (DOH) of the cement clinker phases (C_3S, C_2S, C_3A, and C_4AF) at a given age (denoted as DOR_{ph}), which is the mass fraction of the clinker phase available to react at a given time. The mass fraction of minor oxides in the cement (Na_2O, K_2O, MgO, and SO_3) is determined from the degree of clinker hydration following the method outlined in Taylor.[67] The DOH of the system at a given age is the mass normalized DOR_{ph} of the four clinker phases.

Pore partitioning model

Thermodynamic modeling can only provide the total amount of liquid water in the OPC paste after the hydration reaction occurs. Recent works[38-40] have shown that thermodynamic models can be synergistically combined with the concepts of the Powers-Brownyard model[68] using a PPM to calculate the volume fraction of gel solids, gel pores (pores less than 5 nm in size[40]), capillary pores (pores between 5 nm and a few μm in size[40]), and pores due to chemical shrinkage that are present in the OPC systems. The PPM has been successfully used to predict the porosity and pore volumes of OPC pastes.[38] The PPM has been extended to OPC mortar and concrete materials to predict the total porosity and several porosity-related performance properties using a pore partitioning model for concrete (PPMC).[17,40]

The total porosity of the paste (ϕ_p in vol. %) is calculated as the sum of the volume fractions of gel water (v_{gw}), capillary water (v_{cw}), and pores due to chemical shrinkage (v_{cs}), as shown in Eq. (1)

$$\phi_p = v_{gw} + v_{cw} + v_{cs} \tag{1}$$

The porosity of the paste can be scaled up to calculate the porosity of the mortar system (ϕ_m) using the PPMC[17] using the volume fraction of paste in the mortar (V_p), the volume fraction of the air voids (V_{air}), and the volume fraction of aggregates (V_{agg}), as shown in Eq. (2)

$$\phi_m = V_p \phi_p + V_{air} + V_{agg} \phi_{agg} \tag{2}$$

where ϕ_{agg} is the porosity of the aggregate (in vol. % of the aggregate).

Property-porosity relations

The third step of the framework uses property-porosity relations to predict the mechanical properties of the paste—that is, E_p, G_p^c, and f_{tp}'. The pore volumes and distribution of hydration products are parameters that affect the mechanical and fracture properties.[69] A higher porosity in OPC systems typically means a lower load-carrying capacity due to the lower volume of hydrates. Pores can also act as stress concentration sites in the hydrated OPC paste and promote failure under loading by introducing microcracks. Hence,

increasing the porosity of the paste reduces the material's elastic modulus, strength, and fracture energy.[70]

A model proposed by Jelitto and Schneider[61,62] that incorporates the porosity and the distribution of solids is used to predict the mechanical properties of the paste assuming an open porous microstructure (when all the pores are connected and some of the solid hydration products [the load-carrying phases] are connected, with some disconnections; refer to Fig. 3 in Jelitto and Schneider[61] for a schematic of the model).

The E_p and G_p^c is calculated using Eq. (3) and (4), respectively

$$\frac{E_p}{E_p^{\phi=0}} = \left(\frac{1-d}{d^2} + \frac{1}{3d - 2d^2}\right)^{-1} \left(1 - \phi_p\right)^n \tag{3}$$

$$\frac{G_p^c}{G_p^{\phi=0}} = d^2 \left(1 - \phi_p\right)^n \tag{4}$$

where ϕ_p is the paste porosity (calculated using Eq. (1)); $E_p^{\phi=0}$ and $G_p^{\phi=0}$ are the elastic modulus and fracture energy of the paste at a hypothetical state of zero porosity; and d is a geometric parameter of the paste microstructure calculated using Eq. (5)

$$d = \cos\left(\frac{2\pi - \cos\left(2\phi_p - 1\right)^{-1}}{3}\right) + \frac{1}{2} \tag{5}$$

The values of $E_p^{\phi=0}$ are calculated using the rule of mixtures (using the series model to obtain the lower bound) and is calculated as shown in Eq. (6)

$$E_p^{\phi=0} = \frac{E_{gel} E_{ub}}{v_{gel}' E_{ub} + v_{ub}' E_{gel}} \tag{6}$$

where E_{gel} is the elastic modulus of the hydrated gel phase (considered to be 29.25 GPa[47]); E_{ub} is the elastic modulus of the unhydrated clinker grains (considered to be 139.90 GPa[47]); v_{ub}' is the volume of unhydrated clinker in the hypothetical zero-porosity system; and v_{gel}' is the volume of the gel phase in the hypothetical zero-porosity system. The values of v_{ub}' and v_{gel}' are calculated using Eq. (7) and (8), respectively

$$v_{ub}' = \frac{v_{ub}}{v_{ub} + v_{gw} + v_{gs}} \tag{7}$$

$$v_{gel}' = \frac{v_{gw} + v_{gs}}{v_{ub} + v_{gw} + v_{gs}} \tag{8}$$

The f_{tp}' can be computed assuming cement paste is an ideal brittle material with a single crack using Eq. (9).

$$f_{tp}' = \left(\frac{E_p \cdot G_p^c}{\pi a}\right)^{0.5} \tag{9}$$

where f_{tp}' is the strength of the paste; and a is half the internal crack length.

In general, LEFM can be considered as a good approximation for cementitious pastes when the crack size is larger than 1 mm.[71] However, for smaller-length scales, the Griffith equation tends to overestimate the flexural strength of ordinary cement paste.[71] As the crack length and representative volume decreases, the characteristic fracture length scale becomes relevant, and other considerations should be considered.[54] While in this work the initial crack size was calculated to be 0.3 mm from the ball-on-three-balls (B3B) experiments, a statistical approach is also used that takes into account the variability in the defect size and distribution of defects using a Weibull distribution of tensile strength and fracture energy in the finite element analysis (FEA) model.

FEA-based mechanical model for heterogenous materials

In the fourth step, two-dimensional FEA models[54] are created to study the tensile strength development of mortar composites (refer to Fig. 1, block 4) using mechanical properties for the paste matrix determined from the previous step, along with the morphological and mechanical characteristics of the aggregate and interfacial transition zone (ITZ). This model integrates a continuum-based finite element approach and a bilinear cohesive zone model to predict the resulting tensile strength of mortar beams. The cohesive zone model introduces the nonlinear fracture mechanics concepts to the simulation to predict the fracture behavior of quasi-brittle materials,[72-74] representing a progressive damage zone behind the crack tip. The interface elements are inserted between the bulk elements to transfer the normal and tangential forces until debonding. For instance, a two-dimensional boundary value problem of the mortar representative volume element is shown in Fig. 2(a). Schematics of three sets of interface elements inserted within fine aggregate particles, the cement paste matrix, and their interface are shown in Fig. 2(b). The cohesive interface law describes the evolution of tensile and shear tractions in terms of both normal and tangential displacement jumps within interface elements.

The normal tensile and shear traction at the interface is determined from the cohesive interface law. The nodal forces in the plane of the element are computed from the known interface traction as $T' = \int_S N_S^T t dS$, where T' is the force vector (T_n and T_t); t is the computed interface traction vector (t_n and t_t); and N_s is the shape function vector; all quantities are defined in the local coordinates of the element. The cohesive law for interface elements is formulated in terms of normal and shear components of stresses $\sigma = (T_n, T_t)$ on the interface element and corresponding relative displacements $u = (u_n, u_t)$, shown in Fig. 2(c) and (d). A bilinear cohesive law in opening and shear modes is implemented using the finite element package Abaqus.[75] Readers are referred to Esmaeeli et al.[54] for further detailed information on the multiscale cohesive law development for cementitious systems. A Weibull strength distribution is used to account for: 1) the presence of preexisting defects in the material; and 2) the fact that these defects are smaller than 1 mm, and this is discussed in detail in the "Results and Discussion" section.

MODEL VALIDATION

This study uses the modeling framework of experiments to calibrate and validate the E_p, G_p^c, and f_{tp}' calculated using Eq. (3), (4), and (9), and the tensile strength of mortar (f_{tm}') predicted by the FEM. The E_p, f_{tp}', and f_{tm}' were measured experimentally for OPC pastes and mortars across a wide range of porosities. Experimental data from the literature was also used to validate the model predictions for E_p and G_p^c. Five paste and one mortar samples are prepared for each target porosity. Table 1 depicts the mixture proportions for paste and mortar samples for each target paste porosity. Note that the water-binder ratio (w/b) and curing durations for the mixtures were selected using the outputs of the PPM to achieve a target porosity. A Type I/II cement was used (53% C_3S, 17% C_2S, 7% C_3A, 9% C_4AF, 0.62% Na_2O_{eq}, 3.8% MgO, 3% $CaCO_3$, and 2.8% SO_3).

Preparing paste cylinders

Five cylinders of 50 mm diameter and 100 mm length were cast to measure the E_p using ultrasonic pulse velocity (UPV) and f_{tp}' using the B3B test. The pastes were cast following a modified version of ASTM C305-20,[76] outlined in Bharadwaj et al.[40] and Fu and Weiss.[77] The cement was added to the mixing bowl and thoroughly dispersed by dry mixing in a vacuum mixer (203 mbar = 80% vacuum) at 300 rotations per minute (rpm) for 90 seconds. Next, water was added and the cement and water were mixed for 90 seconds at 300 rpm. The mixer was then stopped for a 15-second rest period, during which the material collected on the sides of the mixing bowl and paddle were scraped back into the bulk of the mixing bowl. After the rest period, the wet paste was then mixed for another 90 seconds at 400 rpm. After the mixing, the fresh paste was cast into polyurethane molds, vibrated to remove the air (care was taken to prevent excessive bleeding), and sealed using plastic film and duct tape to prevent the loss of moisture. The molds containing the fresh paste were rotated for 24 hours after casting to minimize bleeding. After 24 hours, the samples were double-bagged to prevent moisture loss and sealed-cured at 23 ± 2°C until the testing age.

Preparing mortar cylinders and prisms

The mortar was mixed following the procedure outlined in ASTM C305-20.[76] Natural river sand with a maximum size of 4.75 mm (passing No. 4 sieve) was used in this work. The sand had a specific gravity of 2.65 and an absorption capacity of 2.7%. More details about the sand can be found in Bharadwaj et al.[16] The sand was used in its saturated surface-dry state to not change the w/b of the mixture. The fresh mortar was placed in prism molds which were pre-coated with a release agent. For this study, prisms of 125 x 25 x 25 mm were cast. The mortar-filled molds were vibrated to minimize entrapped air within the sample, and care was taken to prevent excessive segregation. The molds were covered with plastic wrap to minimize evaporation and allowed to harden for 24 hours. After 24 hours, the prisms were demolded and cured in saturated lime solution until the testing age.
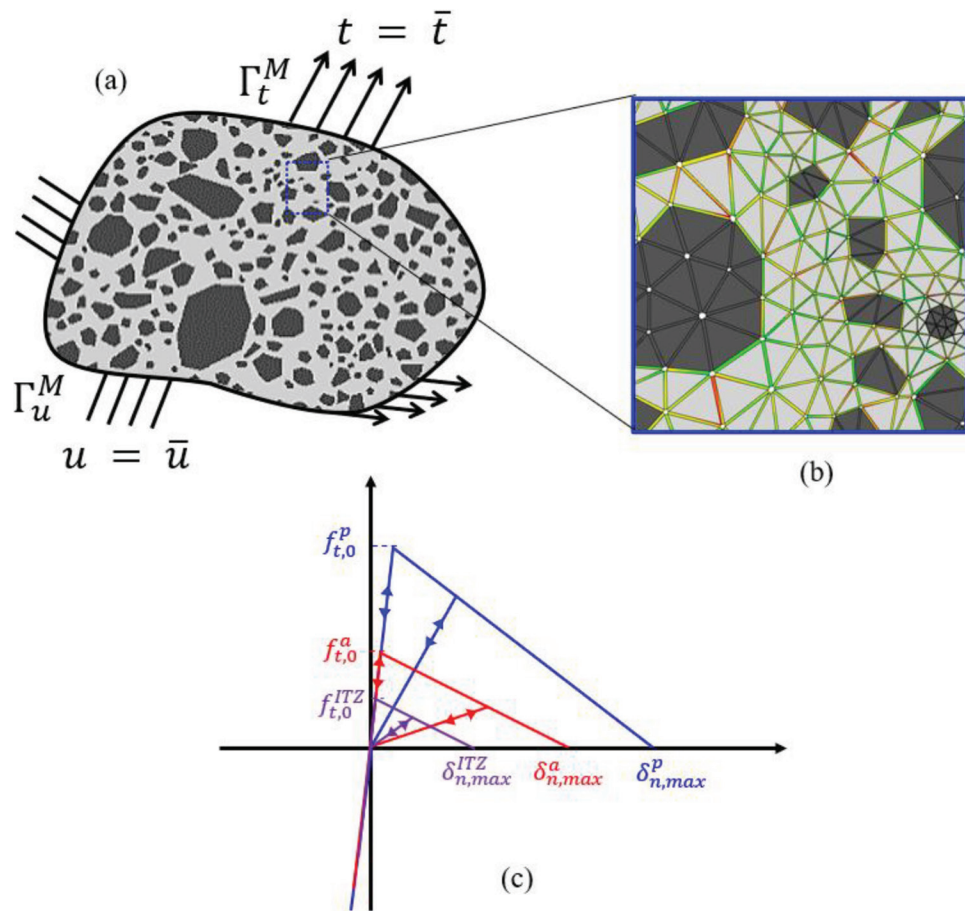
Fig. 2—Schematic representation of two-dimensional mesostructure of heterogeneous cementitious material: (a) under mixed-mode loading. This heterogeneous structure is composed of: (b) continuum bulk elements for paste and aggregate, and interface elements for paste, aggregate, and ITZ, with cohesive law defined in: (c) cohesive opening model.

Table 1—Mixture proportions of paste and mortar mixtures

Name	w/b	Target $\phi_p{}^*$	Curing time, days	Cement, kg/m^3	Water, kg/m^3	Sand, kg/m^3
Paste						
P-30	0.35	30%	56	1498	524	—
P-35	0.40	35%	56	1394	558	—
P-40	0.50	40%	56	1223	612	—
P-45	0.50	45%	10	1223	612	—
P-50	0.60	50%	10	1090	654	—
P-60	0.65	60%	3	1034	672	—
Mortar[†]						
M-45	0.50	45%	10	612	306	1361

[*]ϕ_p are rounded to nearest 5%.

[†]Mortar samples are 50% paste by volume.

Measurement of elastic modulus using UPV test

At the testing age, the cylinders were demolded and their ends were cut to ensure a flat surface to maximize contact with the UPV equipment. A UPV test kit was used to calculate the time it takes for an ultrasonic pulse to travel across the sample. The length of the sample was measured using vernier calipers, and the velocity of the sound wave through the sample (v_{pulse}) was determined by dividing the measured sample length with the measured pulse time. The elastic modulus of the material (E) was calculated using Eq. (10)[9]

$$E = v_{pulse}^2 \cdot \rho \left(\frac{(1+\upsilon) \cdot (1-2\upsilon)}{1-\upsilon} \right) \quad (10)$$

where ρ is the density of the material (calculated based on the mixture proportions); and υ is the Poisson's ratio of

the material (considered to be 0.29 for pastes and 0.20 for mortars from the literature[77,78]).

Measurement of strength using B3B test

The f_{tp}' was measured using the B3B test using 2.54 mm slices cut from the cylinders using a precision saw. The B3B test is an experimental approach for estimating the tensile strength of a thin disk-shaped sample loaded with the fourth ball from the top opposite the three balls.[77,79-82] Börger et al.[79] stated that this test is free of alignment errors with less than 2% characteristic error. It should be noted that the strength obtained by this is higher than that of beam tests, but this is likely due to size effects. Fu and Weiss[77] suggested that samples tested with an effective volume lower than 100 mm³ for paste samples are unlikely to exhibit a size effect.

The tensile strength of paste material is determined by calculation of maximum principal stress at the center of the disk using Eq. (11)[77]

$$f_{tp}' = \frac{P_{max}}{t^2} \cdot \left[c_0 + \frac{c_1 + c_2 \frac{t}{R} + c_3 \left(\frac{t}{R}\right)^2 + c_4 \left(\frac{t}{R}\right)^3}{1 + c_5 \left(\frac{t}{R}\right)} \times \left(1 + c_6 \left(\frac{R_a}{R}\right)\right) \right]$$

(11)

where R is the radius of the disk (mm); R_a is the radial distance from the center of the disk to the center of the support balls (mm); and c_0 to c_6 are dimensionless constants which are functions of Poisson's ratio and Weibull modulus listed as follows: $c_0 = -16.35$, $c_1 = 20.78$, $c_2 = 622.62$, $c_3 = -76.88$, $c_4 = 50.38$, $c_5 = 33.74$, and $c_6 = 0.06$.

Measurement of strength using three-point bending test

The tensile strength of the mortar prisms (f_{tm}') is measured using the three-point bending (3PB) test following the procedure in ASTM C78/C78M-21.[83] In this study, the tensile strength of one mortar mixture with a w/b of 0.50 cured for 10 days (target paste porosity of 45%) was measured experimentally. A beam of 25.4 mm depth x 25.4 mm width x 125 mm length was tested. The tensile strength of the sample is calculated based on the recorded peak load (P_{peak}), loading span (L), width (B), and thickness (D) of samples using Eq. (12)

$$f_{tm}' = \frac{3P_{peak} \cdot L}{2B \cdot D^2}$$

(12)

RESULTS AND DISCUSSION
Thermodynamic modeling and pore partitioning model

The first two steps of the framework proposed in this paper are the thermodynamic model and PPM, respectively. Figure 3(a) shows the output of the thermodynamic model (that is, volume fractions of reaction products) at the target porosity values. In general, an increase in the porosity is achieved by either an increase in the w/b or a decrease in

the curing age (which translates to a lower overall DOH of the system). Therefore, systems with a higher porosity have a higher volume of pore solution in the system. The volume fraction of the reaction products is also lower in systems with a higher target porosity. The volume of unhydrated cement decreases as the water-cement ratio (w/c) increases at a given age due to an increase in the DOH at a given age (refer to porosity values of 30 to 40% and 45 to 50%). A decrease in the curing time at a given w/b results in the volume fraction of unhydrated cement increasing due to a lower DOH in systems cured for shorter durations (porosity values of 40 to 45% and 50 to 60%).

Figure 3(b) shows the Powers-Brownyard phases of the systems as a function of their target porosity. As the target porosity increases, the volume of capillary water increases as the increase in target porosity is achieved by increasing the w/b and/or reducing curing time. For the same reason, the volume of hydration products, gel solids, and gel pores decrease with increased target porosity.

Property-porosity relations

It is well-established that the pore network of cementitious materials is connected with disconnections existing between some portion of the pores[84] and some portion of the gel solids.[85,86] In the property-porosity relations used (refer to Eq. (3) and (4)), the parameter n is related to the disconnections in the gel solids phase and is estimated by fitting the equation to the experimental measurements of elastic modulus. The E_p obtained from the UPV test is the dynamic modulus, and the static modulus is obtained by scaling down the measured value of E_p by 0.75 based on experimental observations in Trifone[87]; however, it should be noted that the mechanical properties used in this paper are a normalized value (that is, $E_p/E_p^{\phi=0}$), so this scaling is only performed for the experimentally obtained E_p in Fig. 4. Figure 4(a) shows a plot of the model predicted (lines) and experimentally measured (markers) $E_p/E_p^{\phi=0}$ as a function of the paste porosity. From the model predictions, it is seen that an increase in porosity decreases the E_p as there is a higher volume of voids and a lower volume fraction of load-carrying gel solids. At a given porosity, an increase in the parameter n leads to a lower E_p as n indicates the disconnections in the load-bearing phase. In general, the experimental measurements follow the trend of the model predictions, and all but one data point lie within $n = 0.5 \pm 0.15$. The value of $n = 0.5$ is chosen for this work as it fits the experimental data to within 7%.

Figure 4(b) plots $G_p^c/G_p^{c\phi=0}$ as a function of porosity. An increase in porosity leads to a lower G_p^c due to a lower amount of solid material, and an increase in n leads to a lower G_p^c at a given porosity due to an increase in the disconnectivity in the solid phase. The predictions of G_p^c for the limited experimental data from the literature[88,89] is within 3% for $n = 0.5$, supporting the chosen value of n.

Figure 4(c) shows the model predicted f_{tp}' and the experimentally measured f_{tp}'. An increase in the porosity decreases the f_{tp}' as the voids in the paste increase. An increase in n decreases the f_{tp}' as the number of disconnections in the load-bearing hydrate phases increases. The predicted f_{tp}' is within
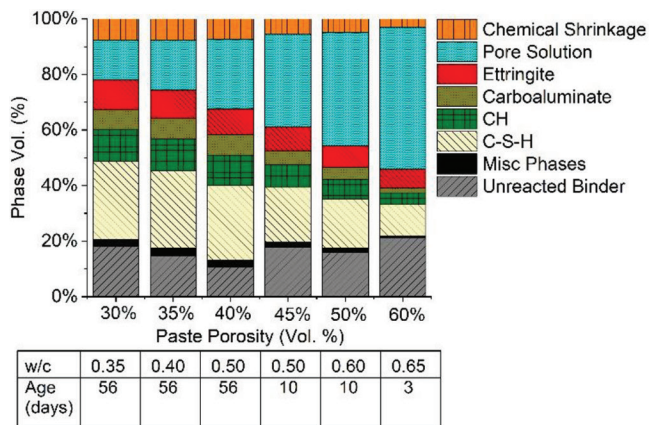
(a)
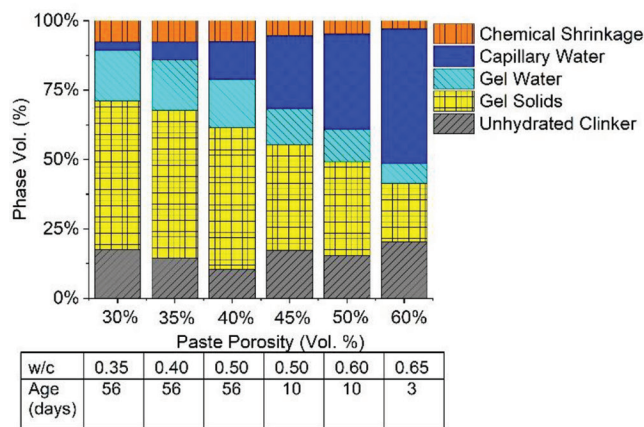
(b)

Fig. 3—Plots of: (a) reaction products; and (b) Powers-Brownyard phases as function of total porosity of paste. (Note: These plots are function of porosity as experiments were designed to capture behavior of property-porosity relations at wide range of porosities.)

2% for $n = 0.5$, supporting the chosen value of n. The deviation of the data point at $\phi_p = 60\%$ from the trend line is likely due to the high w/b and low curing age chosen, resulting in a larger disconnectivity in the load-bearing phases, resulting in a lower E_p and f_{tp}'.

Numerical predictions of mortar

Finite element model—The flexural strength of mortar (f_{tm}') is predicted using a finite element approach. A computational model of the 3PB test is created to predict the f_{tm}'. The boundary conditions are simulated as rigid rollers with frictionless contact between the rollers and the mortar beam (Fig. 5(a)). A plain strain condition is chosen for the model, and the load is applied directly by the top roller, which is subjected to a prescribed displacement (δ). It is considered that the fracture process takes place inside a representative volume element (RVE),[90] which contains the geometry and spatial distribution of different phases. In this study, the RVE contains three phases: cement paste, aggregate, and their ITZ. The mesostructure of the RVE is generated by scanning an optical image of a mortar sample and then importing it as a finite element mesh for the numerical analysis (refer

to Fig. 5(b)). After generating the RVE, the cohesive interface elements are inserted into the model[54] (refer to Fig. 5(c) and (d)). To improve the computational efficiency, the RVE with cohesive interfacial elements is only embedded into the midspan of the mortar beam where the fracture process takes place. It is assumed that the region outside the RVE is free of inelastic deformation, damage, or cracks and is modelled as a continuum material representing the mortar with homogenized properties. To determine the size of the RVE and avoid boundary effects, an RVE size analysis is performed (refer to Appendix A[*] for details).

A Weibull distribution is employed in the FEM to account for the effect of preexisting cracks on the resulting f_{tm}' prediction. It is considered that the preexisting cracks only occur in cement paste and the ITZ and assumed that the aggregate is free of preexisting cracks (that is, f_{tp}', G_p^c, f_{tITZ}', and G_{ITZ}^c have variability in the model). The Weibull distribution for the f_{tp}' is given by Eq. (13),[91] and the form of the Weibull distribution for the other parameters is similar.

$$p\left(f_{tp}'\right) = \frac{m}{f_{tp}'}\left(\frac{f_{tp}}{f_{tp}'}\right)^{m-1}\exp\left[-\left(\frac{f_{tp}}{f_{tp}'}\right)^{m}\right] \quad (13)$$

where f_{tp}' is the nominal strength; and m is the Weibull modulus, which controls the shape of the distribution around f_{tp}'. The value of m for brittle materials, such as mortar and cement paste, can generally take a value between three and 10.[92,93] Figure 6(a) shows an example statistical histogram for the Weibull distribution of f_{tp}' with $m = 5$. Figure 6(b) shows an example where each cohesive element contains a different value of f_{tp} (represented by color map).

Determination of E, f$_t'$, *and* G$_c$—As shown in Fig. 5(a), the region of the mortar prism outside the RVE is modeled as a continuum material. As such, the E, f_t', and G_c of the components of mortar (that is, the cement paste, aggregate, and the ITZ) need to be determined. For the cement paste, aggregate, and ITZ, the E for continuum elements, and the f_t' and G_c for cohesive elements need to be determined. The E_p, G_p^c, and f_{tp}' are calculated from the porosity-properties relations using the values of $n = 0.5$ and $n = 1$. The mechanical properties of the ITZ are difficult to characterize as they are affected by the aggregate surface roughness, aggregate types, and sample curing conditions.[94,95] Experimental results show that the ITZ is typically weaker than the cement paste.[96-100] As such, the f_{tITZ}' and G_{ITZ}^c are a fraction of the f_{tp}' and G_p^c. Following the literature,[96,97] the f_{tITZ}' is 25% of the f_{tp}', and the G_{ITZ}^c is 25% of the G_p^c. The E_{agg}, G_{agg}^c, and f_{tagg}' are obtained from Weiss et al.[98] Table 2 shows an example of the values of the mechanical properties that are used as inputs for the model for one system ($\phi_p = 30\%$). For the systems with other ϕ_p, the properties are obtained in a similar manner.

Influence of Weibull distribution on f$_{tm}'$ *prediction*—After the mechanical properties of the cement paste are
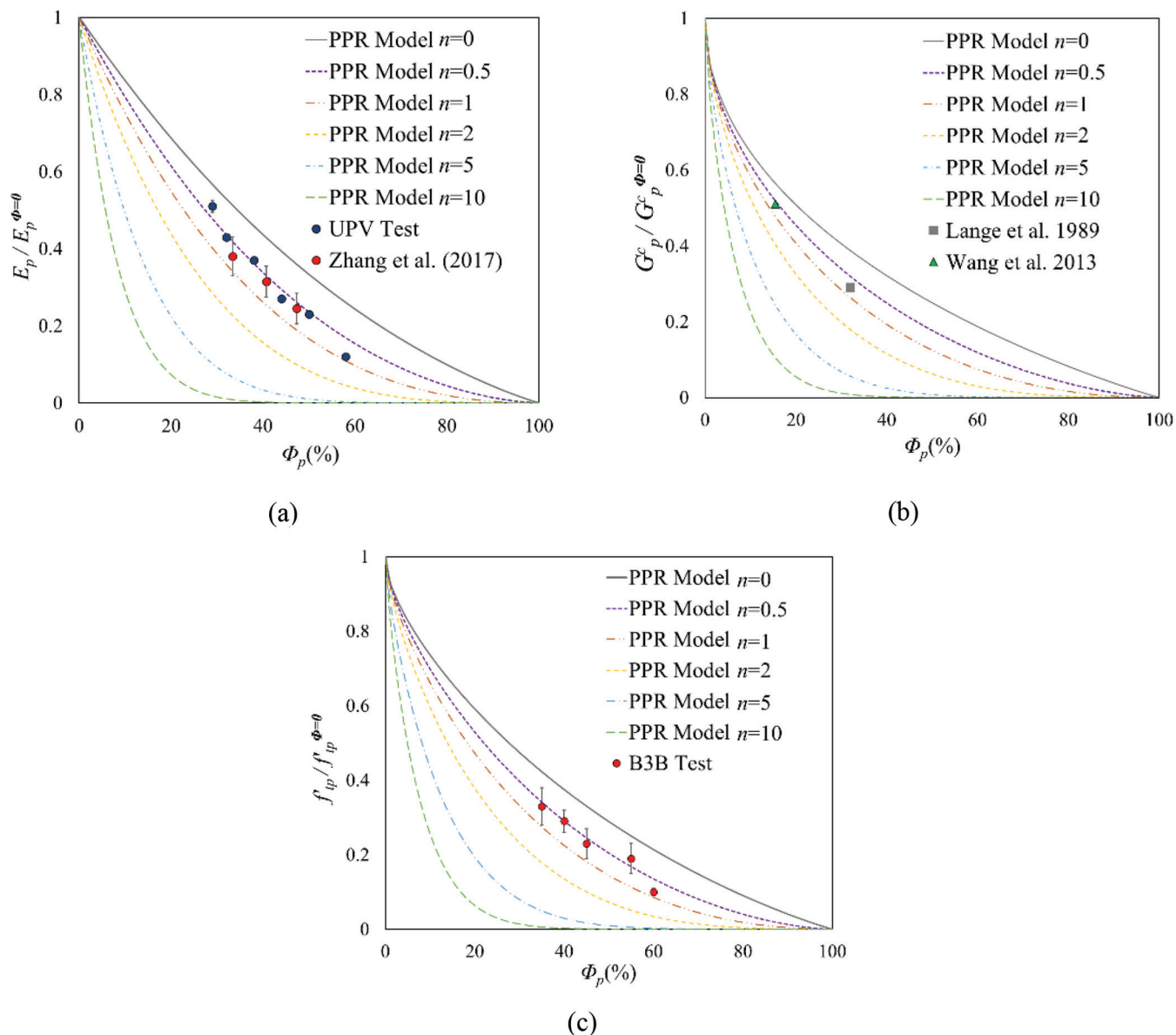
Fig. 4—(a) Elastic modulus; (b) fracture energy; and (c) tensile strength of paste as function of paste porosity.

determined, a Weibull distribution is applied to the cement paste and ITZ strength and fracture energy to represent mortar samples with the same material properties but with random distributions of preexisting cracks. Four models for beams (with dimensions of 25 x 25 x 125 mm³) under a 3PB loading condition are developed with the same RVE, material properties (cement paste with ϕ_p = 30% and n = 1), and Weibull modulus m. The value of m is assumed to be the same for the paste and ITZ and is considered as 5 following Esmaeeli et al.[54] The only difference between these models is the distribution of preexisting cracks in the RVE obtained from Weibull distributions. Figure 7(a) presents the simulation results of flexural stress-deformation curves for these four models. Up to a displacement value of 0.057 mm, all the models overlap; however, the samples failed at different stresses due to the random distribution of preexisting cracks. The model predicts a f_{tm}' of 12.84 ± 0.50 MPa. From the 3PB experiment described in the previous section, the standard deviation in the measured flexural stress is 0.53 MPa, which

is consistent with the numerical prediction. Only the standard deviation of the experimental results and model predictions are compared to validate the variation in the flexural strength prediction caused by the Weibull distribution; the average flexural strength will be discussed in a later section. From Figure 7(b), two crack patterns from the simulations are observed. Similar to the observations on the crack path in the experiment, the cracks propagate in different paths due to the random distribution of preexisting cracks. These consistencies between experiments and simulations support the validity of the model and indicate that m = 5 is appropriate for the f_{tm}' prediction.

Influence of aggregate shape and distribution on f_{tm}' prediction—Three beam models (with dimensions of 25 x 25 x 125 mm³) are studied under 3PB loading conditions to study the influence of aggregate shape and distribution. Studying the influence of aggregate size and minerology on the fracture behavior is outside this paper's scope and can be found in Esmaeeli et al.[106] and Santos et al.[107] Studying the
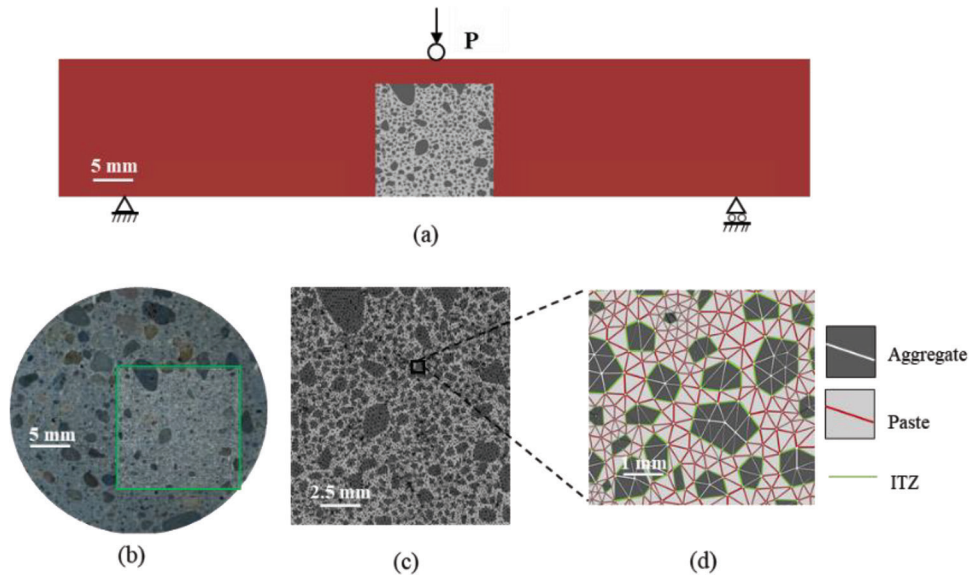
Fig. 5—(a) Schematic of FEM showing loading conditions for 3PB test; (b) optical image of mortar sample and digitized meso-structure of RVE (inset green box; length of white line indicates 5 mm); (c) RVE and FEM mesh; and (d) details of FEM mesh includes aggregates, paste, and ITZ between them. (Full-color PDF can be accessed at www.concrete.org.)

Table 2—Material properties of cement paste, ITZ, and aggregate

Properties	f_t', MPa	G_c, N/mm	E, GPa
Paste, $\phi_p = 30\%$, $n = 0.5$	29.4	0.051	26.9
Paste, $\phi_p = 30\%$, $n = 1$	24.6	0.045	23.9
ITZ, $n = 0.5$	7.3	0.013	—
ITZ, $n = 1$	6.1	0.011	—
Aggregate	9.8	0.120	65.2

applicability of the model with different aggregate mineralogies is scope for future work. The material properties (cement paste with $\phi_p = 30\%$, $n = 1$, and $m = 5$), RVE size (Appendix A), and aggregate volume fraction (Appendix B) are identical for the three beams. Four simulations for each RVE are performed with the same Weibull parameters to account for the random preexisting cracks (indicated by the standard deviation in the f_{tm}' predictions). Figure 8 shows the f_{tm}' predictions, RVEs, and crack patterns in the RVEs. The f_{tm}' predicted for RVE (No. 1), (No. 2), and (No. 3) (which represent three different aggregate shapes and distributions generated) are 12.84 ± 0.50 MPa, 13.49 ± 0.49 MPa, and 12.64 ± 0.64 MPa, respectively. The average f_{tm}' prediction for the three RVEs is 12.99 ± 0.44 MPa. The standard deviation of the experimentally measured f_{tm}' is 0.53 MPa, which is consistent with the numerical prediction. The comparison of the variability indicates that the variation of f_{tm}' prediction due to the different aggregates shape and spatial distribution is reasonable, and the f_{tm}' predictions remain within the margin of experimental accuracy.

f_{tm}' *prediction for mortar with different* ϕ_p—After determining material properties and validating the FEA model framework, the influences of porosity (ϕ_p) on the f_{tm}' predictions are studied. As mentioned in the previous section, 3PB experiments for mortar beams (25 x 25 x 125 mm³ and $\phi_p = 45\%$) were conducted. A model for the same beam is

(a)

(b)
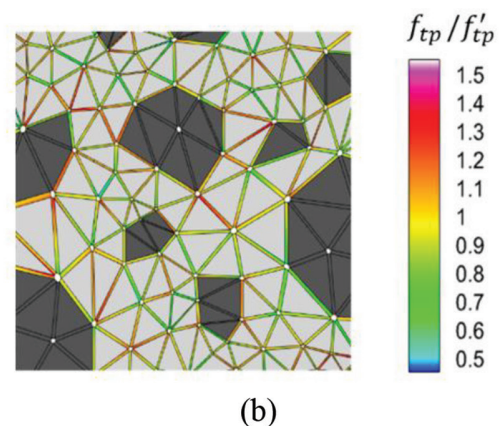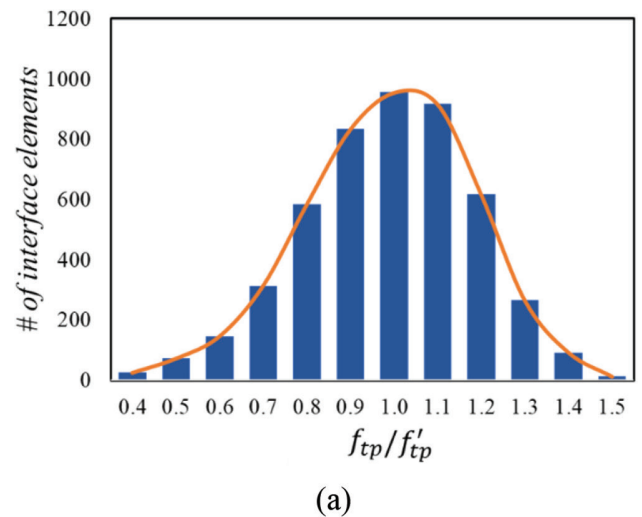
Fig. 6—(a) Histogram for Weibull distribution of f_{tp}' (orange curve represents Eq. (13)); and (b) example of cohesive element strength distribution (triangular continuum elements were shrunk for illustration purposes). Color map represents f_{tp}/f_{tp}' values. (Full-color pdf can be accessed at www.concrete.org.)
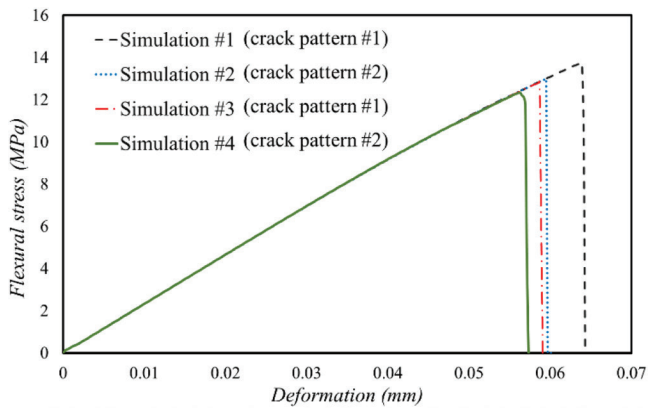
(a)
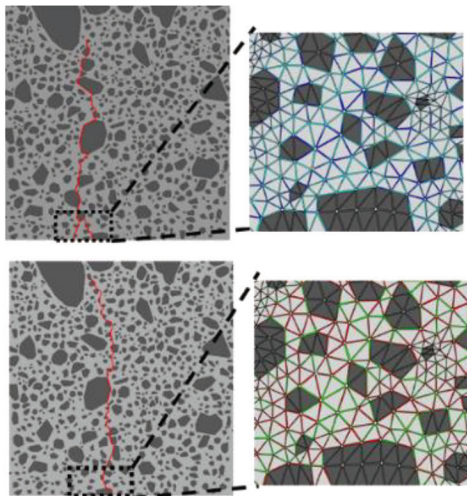
(b)

Fig. 7—(a) Simulation results of flexural stress versus defor-mation curves for samples with same material parameters but random distribution of preexisting cracks; and (b) two crack patterns due to random distribution of preexisting cracks. Color maps represent random distribution of preex-isting cracks (crack pattern No. 1 on top; crack pattern No. 2 on bottom). (Full-color PDF can be accessed at www.concrete.org.)

developed to validate the f_{tm}' prediction. In addition, simu-lations for mortar beams with ϕ_p of 30, 39, and 55% are also performed to investigate the influence of ϕ_p on f_{tm}'. The model is run for two values of the disconnection parameter n ($n = 0.50$ and $n = 1$) to simulate the typically observed range of n in OPC pastes.

Figure 9 presents the f_{tm}' predictions and the experiment results for mortar beams with different ϕ_p. The measured f_{tm}' at $\phi_p = 45\%$ is 8.44 ± 0.53 MPa and the f_{tm}' predicted by the model is 9.69 ± 0.21 MPa (for $n = 0.5$). The range of experimental f_{tm}' (7.72 to 9.43 MPa) lies within the exper-imental margin of error (±1.5 MPa) to the model predicted f_{tm}' (9.33 to 9.87 MPa). Two data points from the litera-ture[101,102] are also plotted. The data point at $\phi_p = 52\% \pm 2\%$ is closer to the $n = 1$ model curve, likely due to the early age of testing (3 days), resulting in a higher n. From the f_{tm}' predictions results, it can be observed that as the ϕ_p of the
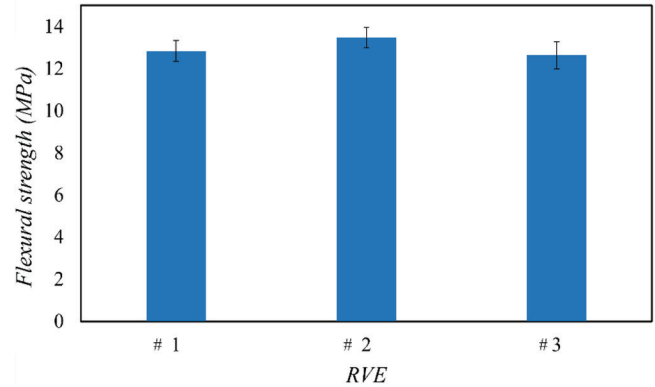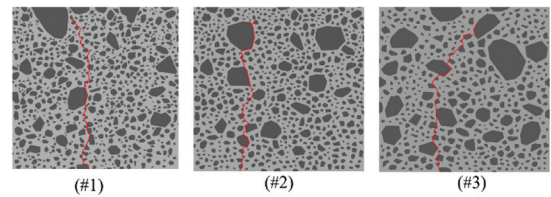
Fig. 8—Flexural strength predictions and crack patterns from three RVEs with different aggregate shape and distribution.
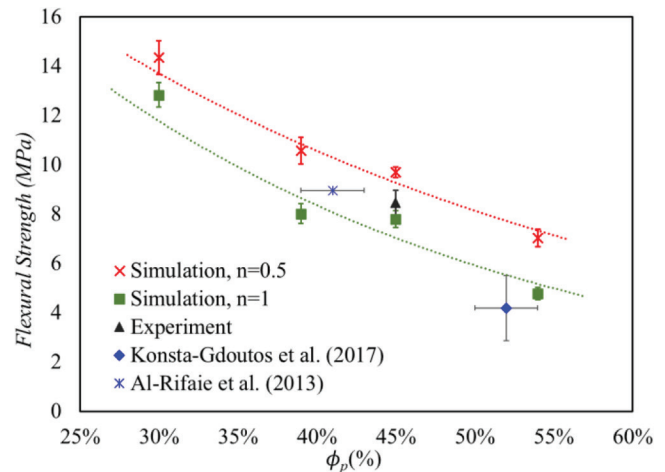
Fig. 9—Experiment and simulation results for mortar beams with different ϕ_p; red and greed dashed lines are trend lines of simulation predictions with two values of disconnection parameter n (n = 0.50 and n = 1). (Note: Trend lines are intended to be visual guides; full-color PDF can be accessed at www.concrete.org.)

mortar increases, the f_{tm}' of the mortar decreases, which is consistent with results from the literature.[99,103] The results suggest that the modeling can capture the influence of paste porosity (predicted from thermodynamic modeling) on the f_{tm}' development. The data to support each step of the model is in the typical range of ϕ_p seen in concrete (30 to 55%) and obtaining data beyond this range is scope for future work.

CONCLUSIONS
This paper described a four-step approach to predict the mechanical response of ordinary portland cement (OPC) systems. The first step in this process is the use of a ther-modynamic model to predict the reaction products of the hydration reaction. The second step is using the results of

thermodynamic modeling as inputs to using a pore partitioning model (PPM) to predict the porosity and pore volumes (volumes of gel pores, capillary pores, and pores due to chemical shrinkage) in the hydrated paste. The third step calculates property-porosity relations to predict the mechanical properties of the paste—that is, the E_p, G_p^c, and f_{tp}' as a function of the porosity. The disconnections in the hydrated gel solids (that is, the n value) is calibrated using experimental data, and using the value of n, the G_p^c and f_{tp}' are predicted. The fourth step in this paper is the use of finite element models (FEMs) to predict the mechanical behavior of mortars made with the OPC using the mechanical properties of the paste (from step 3) as the inputs. The model is run for two values of the disconnection parameter n (n = 0.50 and n = 1) to simulate the typically observed range of n in OPC pastes; the model predictions (7.54 ± 0.35 MPa to 9.69 ± 0.21 MPa) are similar to the experimental measurements (8.44 ± 0.53 MPa) for the mortar beam with ϕ_p = 45%, within the margin of experimental error. This four-step approach natively considers the binder chemistry to predict the mechanical response of cementitious pastes and concrete. It can be coupled with a performance-based mixture design framework[8] to natively predict the concrete's flexural strength. Overall, this work is a step toward self-sufficient models that predict concrete performance,[45] which can be used as tools to better design low-carbon concrete.

AUTHOR BIOS

ACI member **Yu Wang** *is a PhD Student in the Lyles School of Civil Engineering at Purdue University, West Lafayette, IN. He received his BS in hydraulic and hydropower engineering from Northwest A&F University, Xianyang, Shaanxi, China, and his MS in civil engineering from Northwestern University, Evanston, IL. His research interests include multi-scale concrete numerical simulations, fiber-reinforced cementitious composite, and architected cement-based material for three-dimensional (3-D) printing.*

ACI member **Keshav Bharadwaj** *is a Postdoctoral Scholar at Oregon State University, Corvallis, OR, where he also received his PhD in civil engineering. His research interests include thermodynamic modeling, reactivity, transport in cementitious systems, and linking the microstructure of concrete to the engineering performance of concrete.*

Hadi S. Esmaeeli *performed this work as a Postdoctoral Researcher at Purdue University, where he also received his PhD. His research interests include bio-inspired design and development of architected materials using novel additive manufacturing processes, and automated robotic technologies for applications in civil infrastructures.*

Pablo D. Zavattieri *is the Jerry M. and Lynda T. Engelhardt Professor in Civil Engineering at Purdue University, where he also received his PhD. His research interests include the interface between solid mechanics and materials engineering, and bio-inspired and architected materials.*

O. Burkan Isgor, *FACI, is a Professor in the School of Civil and Construction Engineering at Oregon State University. He is Chair of ACI Committee 222, Corrosion of Metals in Concrete, and a member of ACI Committees 236, Material Science of Concrete; and 365, Service Life Prediction. His research interests include corrosion of steel in concrete, service-life modeling, and nondestructive testing.*

W. Jason Weiss, *FACI, is the Edwards Distinguished Professor of Engineering in the School of Civil and Construction Engineering at Oregon State University. He is Editor in Chief of the* ACI Materials Journal *and a Member of the ACI Board of Direction.*

ACKNOWLEDGMENTS

REFERENCES

1. UN Environment, Scrivener, K. L.; John, V. M.; and Gartner, E. M., "Eco-Efficient Cements: Potential Economically Viable Solutions for a Low-CO_2 Cement-Based Materials Industry," *Cement and Concrete Research*, V. 114, 2018, pp. 2-26. doi: 10.1016/j.cemconres.2018.03.015

2. Miller, S. A.; John, V. M.; Pacca, S. A.; and Horvath, A., "Carbon Dioxide Reduction Potential in the Global Cement Industry By 2050," *Cement and Concrete Research*, V. 114, 2018, pp. 115-124. doi: 10.1016/j.cemconres.2017.08.026

3. Juenger, M.; Provis, J. L.; Elsen, J.; Matthes, W.; Hooton, R. D.; Duchesne, J.; Courard, L.; He, H.; Michel, F.; Snellings, R.; and De Belie, N., "Supplementary Cementitious Materials for Concrete: Characterization Needs," *MRS Online Proceedings Library*, V. 1488, 2012, pp. 8-22.

4. Juenger, M. C. G.; Winnefeld, F.; Provis, J. L.; and Ideker, J. H., "Advances in Alternative Cementitious Binders," *Cement and Concrete Research*, V. 41, No. 12, 2011, pp. 1232-1243. doi: 10.1016/j.cemconres.2010.11.012

5. Juenger, M. C. G.; Snellings, R.; and Bernal, S. A., "Supplementary Cementitious Materials: New Sources, Characterization, and Performance Insights," *Cement and Concrete Research*, V. 122, 2019, pp. 257-273. doi: 10.1016/j.cemconres.2019.05.008

6. Lothenbach, B.; Scrivener, K.; and Hooton, R. D., "Supplementary Cementitious Materials," *Cement and Concrete Research*, V. 41, No. 12, 2011, pp. 1244-1256. doi: 10.1016/j.cemconres.2010.12.001

7. Tennis, P. D.; Thomas, M. D. A.; and Weiss, W. J., "State-of-the-Art Report on Use of Limestone in Cements at Levels of Up to 15%," PCA R&D SN3148, Portland Cement Association, Skokie, IL, 2011, 78 pp.

8. Bharadwaj, K.; Isgor, O. B.; Weiss, J. W.; Chopperla, K. S. T.; Choudhary, A.; Vasudevan, G. D.; Glosser, D.; Ideker, J. H.; and Trejo, D., "A New Mixture Proportioning Method for Performance-Based Concrete," *ACI Materials Journal*, V. 119, No. 2, Mar. 2022, pp. 207-220.

9. Mehta, P. K., and Monteiro, P. J. M., *Concrete: Microstructure, Properties, and Materials*, McGraw Hill, New York, 2006, 684 pp.

10. Mindess, S.; Young, J. F.; and Darwin, D., *Concrete*, second edition, Pearson Education, Inc., Hoboken, NJ, 2003, 657 pp.

11. de Larrard, F., *Concrete Mixture Proportioning: A Scientific Approach*, CRC Press, New York, 1999, 448 pp.

12. ACI Committee 211, "Standard Practice for Selecting Proportions for Normal, Heavyweight, and Mass Concrete (ACI 211.1-91) (Reapproved 2009)," American Concrete Institute, Farmington Hills, MI, 1991, 38 pp.

13. Thomas, M., "Optimizing the Use of Fly Ash in Concrete," Publication IS548, Portland Cement Association, Skokie, IL, 2007, 24 pp.

14. Thomas M., *Supplementary Cementing Materials in Concrete*, CRC Press, Boca Raton, FL, 2013, 210 pp.

15. Zajac, M.; Skocek, J.; Adu-Amankwah, S.; Black, L.; and Haha, M. B., "Impact of Microstructure on the Performance of Composite Cements: Why Higher Total Porosity Can Result in Higher Strength," *Cement and Concrete Composites*, V. 90, 2018, pp. 178-192. doi: 10.1016/j.cemconcomp.2018.03.023

16. Bharadwaj, K.; Chopperla, K. S. T.; Choudhary, A.; Glosser, D.; Ghantous, R. M.; Vasudevan, G. D.; Ideker, J. H.; Isgor, O. B.; Trejo, D.; and Weiss, W. J., "CALTRANS: Impact of the Use of Portland-Limestone Cement on Concrete Performance as Plain or Reinforced Material - Final Report," Oregon State University, Corvallis, OR, 2021, 320 pp., https://ir.library.oregonstate.edu/concern/articles/7h149x67f. (last accessed Feb. 16, 2023)

17. Bharadwaj, K.; Glosser, D.; Moradllo, M. K.; Isgor, O. B.; and Weiss, W. J., "Toward the Prediction of Pore Volumes and Freeze-Thaw Performance of Concrete Using Thermodynamic Modelling," *Cement and Concrete Research*, V. 124, 2019, Article No. 105820. doi: 10.1016/j.cemconres.2019.105820

18. Lam, L.; Wong, Y.; and Poon, C. S., "Degree of Hydration and Gel/Space Ratio of High-Volume Fly Ash/Cement Systems," *Cement and Concrete Research*, V. 30, No. 5, 2000, pp. 747-756. doi: 10.1016/S0008-8846(00)00213-1

19. American Coal Ash Association, "Ash at Work: Applications, Science, and Sustainability of Coal Ash," Farmington Hills, MI, 2020, 199 pp.

20. Isgor, O. B.; Ideker, J.; Trejo, D.; Weiss, J. W.; Bharadwaj, K.; Choudhary, A.; Teja, C. K. S.; Glosser, D.; and Vasudevan, G., "Development of a Performance-Based Mixture Proportioning Procedure for Concrete

Incorporating Off-Spec Fly Ash," Report No. 000000003002018795, Energy Power Research Institute (EPRI), Palo Alto, CA, 2020, 78 pp.

21. Bahurudeen, A.; Kanraj, D.; Dev, V. G.; and Santhanam, M., "Performance Evaluation of Sugarcane Bagasse Ash Blended Cement in Concrete," *Cement and Concrete Composites*, V. 59, 2015, pp. 77-88. doi: 10.1016/j.cemconcomp.2015.03.004

22. Bahurudeen, A.; Marckson, A. V.; Kishore, A.; and Santhanam, M., "Development of Sugarcane Bagasse Ash Based Portland Pozzolana Cement and Evaluation of Compatibility With Superplasticizers," *Construction and Building Materials*, V. 68, 2014, pp. 465-475. doi: 10.1016/j.conbuildmat.2014.07.013

23. Bahurudeen, A., and Santhanam, M., "Influence of Different Processing Methods on the Pozzolanic Performance of Sugarcane Bagasse Ash," *Cement and Concrete Composites*, V. 56, 2015, pp. 32-45. doi: 10.1016/j.cemconcomp.2014.11.002

24. Clavier, K. A.; Paris, J. M.; Ferraro, C. C.; and Townsend, T. G., "Opportunities and Challenges Associated With Using Municipal Waste Incineration Ash as a Raw Ingredient in Cement Production–A Review," *Resources, Conservation and Recycling*, V. 160, 2020, Article No. 104888. doi: 10.1016/j.resconrec.2020.104888

25. Hogan, F. J., and Meusel, J. W., "Evaluation for Durability and Strength Development of a Ground Granulated Blast Furnace Slag," *Cement, Concrete and Aggregates*, V. 3, No. 1, 1981, pp. 40-52. doi: 10.1520/CCA10201J

26. Seraj, S.; Cano, R.; Ferron, R. D.; and Juenger, M. C. G., "The Role of Particle Size on the Performance of Pumice as a Supplementary Cementitious Material," *Cement and Concrete Composites*, V. 80, 2017, pp. 135-142. doi: 10.1016/j.cemconcomp.2017.03.009

27. Diaz-Loya, I.; Juenger, M.; Seraj, S.; and Minkara, R., "Extending Supplementary Cementitious Material Resources: Reclaimed and Remediated Fly Ash and Natural Pozzolans," *Cement and Concrete Composites*, V. 101, 2019, pp. 44-51. doi: 10.1016/j.cemconcomp.2017.06.011

28. Kalina, R. D.; Al-Shmaisani, S.; Ferron, R. D.; and Juenger, M. C. G., "False Positives in ASTM C618 Specifications for Natural Pozzolans," *ACI Materials Journal*, V. 116, No. 1, Jan. 2019, pp. 165-172. doi: 10.14359/51712243

29. Seraj, S., "Evaluating Natural Pozzolans for Use as Alternative Supplementary Cementitious Materials in Concrete," PhD thesis, The University of Texas at Austin, Austin, TX, 2014, 176 pp.

30. Kulik, D. A.; Miron, G. D.; and Lothenbach, B., "A Structurally-Consistent CASH+ Sublattice Solid Solution Model For Fully Hydrated C-S-H Phases: Thermodynamic Basis, Methods, and Ca-Si-H$_2$O Core Sub-Model," *Cement and Concrete Research*, V. 151, 2022, Article No. 106585. doi: 10.1016/j.cemconres.2021.106585

31. Lothenbach, B., and Gruskovnjak, A., "Hydration of Alkali-Activated Slag: Thermodynamic Modelling," *Advances in Cement Research*, V. 19, No. 2, 2007, pp. 81-92. doi: 10.1680/adcr.2007.19.2.81

32. Lothenbach, B.; Kulik, D. A.; Matschei, T.; Balonis, M.; Baquerizo, L.; Dilnesa, B.; Miron, G. D.; and Myers, R. J., "Cemdata18: A Chemical Thermodynamic Database for Hydrated Portland Cements and Alkali-Activated Materials," *Cement and Concrete Research*, V. 115, 2019, pp. 472-506. doi: 10.1016/j.cemconres.2018.04.018

33. Lothenbach, B.; Matschei, T.; Möschner, G.; and Glasser, F. P., "Thermodynamic Modelling of the Effect of Temperature on the Hydration and Porosity of Portland Cement," *Cement and Concrete Research*, V. 38, No. 1, 2008, pp. 1-18. doi: 10.1016/j.cemconres.2007.08.017

34. Lothenbach, B., and Winnefeld, F., "Thermodynamic Modelling of the Hydration of Portland Cement," *Cement and Concrete Research*, V. 36, No. 2, 2006, pp. 209-226. doi: 10.1016/j.cemconres.2005.03.001

35. Lothenbach, B., and Zajac, M., "Application of Thermodynamic Modelling to Hydrated Cements," *Cement and Concrete Research*, V. 123, 2019, Article No. 105779.

36. Myers, R. J.; Bernal, S. A.; and Provis, J. L., "A Thermodynamic Model for C-(N-)A-S-H Gel: CNASH_ss. Derivation and Validation," *Cement and Concrete Research*, V. 66, 2014, pp. 27-47. doi: 10.1016/j.cemconres.2014.07.005

37. Myers, R. J.; Lothenbach, B.; Bernal, S. A.; and Provis, J. L., "Thermodynamic Modelling of Alkali-Activated Slag Cements," *Applied Geochemistry*, V. 61, 2015, pp. 233-247. doi: 10.1016/j.apgeochem.2015.06.006

38. Azad, V. J.; Suraneni, P.; Isgor, O.; and Weiss, W. J., "Interpreting the Pore Structure of Hydrating Cement Phases Through a Synergistic Use of the Powers-Brownyard Model, Hydration Kinetics, and Thermodynamic Calculations," *Advances in Civil Engineering Materials*, V. 6, No. 1, 2017, pp. 1-16.

39. Glosser, D.; Azad, V. J.; Suraneni, P.; Isgor, O. B.; and Weiss, W. J., "An Extension of the Powers-Brownyard Model to Pastes Containing Supplementary Cementitious Materials," *ACI Materials Journal*, V. 116, No. 5, Sept. 2019, pp. 205-216. doi: 10.14359/51714466

40. Bharadwaj, K.; Ghantous, R. M.; Sahan, F.; Isgor, O. B.; and Weiss, W. J., "Predicting Pore Volume, Compressive Strength, Pore Connectivity, and Formation Factor in Cementitious Pastes Containing Fly Ash," *Cement and Concrete Composites*, V. 122, 2021, Article No. 104113. doi: 10.1016/j.cemconcomp.2021.104113

41. Bharadwaj, K.; Ghantous, R. M.; Sahan, F. N.; Isgor, O. B.; and Weiss, W. J., "Toward the Prediction of Pore Volumes and Compressive Strength of Concrete Using Thermodynamic Modelling," 6th International Conference on Construction Materials, Fukuoka, Japan, 2020.

42. Bharadwaj, K.; Isgor, O. B.; and Weiss, W. J., "Interpretation of the Results of the Pozzolanic Reactivity Test for Supplementary Cementitious Materials: Insights From Thermodynamic Modeling," *Cement and Concrete Composites*, 2022. (in review)

43. Bharadwaj, K.; Isgor, O. B.; and Weiss, W. J., "A Simplified Approach to Determine the Pozzolanic Reactivity of Commercial Supplementary Cementitious Materials," *Concrete International*, V. 44, No. 1, Jan. 2022, pp. 27-32.

44. Suraneni, P., and Weiss, J., "Examining the Pozzolanicity of Supplementary Cementitious Materials Using Isothermal Calorimetry and Thermogravimetric Analysis," *Cement and Concrete Composites*, V. 83, 2017, pp. 273-278. doi: 10.1016/j.cemconcomp.2017.07.009

45. Isgor, O. B., and Weiss, W. J., "A Nearly Self-Sufficient Framework for Modelling Reactive-Transport Processes in Concrete," *Materials and Structures*, V. 52, No. 6, 2019, Article No. 130. doi: 10.1617/s11527-019-1422-1

46. Powers, T. C., "Structure and Physical Properties of Hardened Portland Cement Paste," *Journal of the American Ceramic Society*, V. 41, No. 1, 1958, pp. 1-6. doi: 10.1111/j.1151-2916.1958.tb13494.x

47. Pichler, B., and Hellmich, C., "Upscaling Quasi-Brittle Strength of Cement Paste and Mortar: A Multi-Scale Engineering Mechanics Model," *Cement and Concrete Research*, V. 41, No. 5, 2011, pp. 467-476. doi: 10.1016/j.cemconres.2011.01.010

48. Pichler, B.; Hellmich, C.; and Eberhardsteiner, J., "Spherical and Acicular Representation of Hydrates in a Micromechanical Model for Cement Paste: Prediction of Early-Age Elasticity and Strength," *Acta Mechanica*, V. 203, No. 3-4, 2009, pp. 137-162. doi: 10.1007/s00707-008-0007-9

49. Pichler, B.; Hellmich, C.; Eberhardsteiner, J.; Wasserbauer, J.; Termkhajornkit, P.; Barbarulo, R.; and Chanvillard, G., "The Counteracting Effects of Capillary Porosity and of Unhydrated Clinker Grains on the Macroscopic Strength of Hydrating Cement Paste–A Multiscale Model," *Mechanics and Physics of Creep, Shrinkage, and Durability of Concrete: A Tribute to Zdeněk P. Bažant*, U. Franz-Josef, J. M. Hamlin, and R. J.-M. Pellenq, eds., 2013, pp. 40-47.

50. Pichler, B.; Hellmich, C.; Eberhardsteiner, J.; Wasserbauer, J.; Termkhajornkit, P.; Barbarulo, R.; and Chanvillard, G., "Effect of Gel-Space Ratio and Microstructure on Strength of Hydrating Cementitious Materials: An Engineering Micromechanics Approach," *Cement and Concrete Research*, V. 45, 2013, pp. 55-68. doi: 10.1016/j.cemconres.2012.10.019

51. Termkhajornkit, P.; Vu, Q. H.; Barbarulo, R.; Daronnat, S.; and Chanvillard, G., "Dependence of Compressive Strength on Phase Assemblage in Cement Pastes: Beyond Gel–Space Ratio—Experimental Evidence and Micromechanical Modeling," *Cement and Concrete Research*, V. 56, 2014, pp. 1-11. doi: 10.1016/j.cemconres.2013.10.007

52. Princigallo, A.; Lura, P.; van Breugel, K.; and Levita, G., "Early Development of Properties in a Cement Paste: A Numerical and Experimental Study," *Cement and Concrete Research*, V. 33, No. 7, 2003, pp. 1013-1020. doi: 10.1016/S0008-8846(03)00002-4

53. Carpinteri, A., and Accornero, F., "Rotation Versus Curvature Fractal Scaling in Bending Failure," *Physical Mesomechanics*, V. 22, No. 1, 2019, pp. 46-51.

54. Esmaeeli, H. S.; Shishehbor, M.; Weiss, W. J.; and Zavattieri, P. D., "A Two-Step Multiscale Model to Predict Early Age Strength Development of Cementitious Composites Considering Competing Fracture Mechanisms," *Construction and Building Materials*, V. 208, 2019, pp. 577-600.

55. Bažant, Z. P., and Planas, J., *Fracture and Size Effect in Concrete and Other Quasibrittle Materials*, Taylor & Francis, New York, 2019, 640 pp.

56. Lilliu, G., and van Mier, J. G. M., "3D Lattice Type Fracture Model for Concrete," *Engineering Fracture Mechanics*, V. 70, No. 7-8, 2003, pp. 927-941. doi: 10.1016/S0013-7944(02)00158-3

57. Shah, S. P.; Swartz, S. E.; and Ouyang, C., *Fracture Mechanics of Concrete: Applications of Fracture Mechanics to Concrete, Rock and Other Quasi-Brittle Materials*, John Wiley & Sons, Inc., New York, 1995, 588 pp.

58. Wriggers, P., and Moftah, S. O., "Mesoscale Models for Concrete: Homogenisation and Damage Behaviour," *Finite Elements in Analysis and Design*, V. 42, No. 7, 2006, pp. 623-636. doi: 10.1016/j.finel.2005.11.008

59. Lothenbach, B.; Le Saout, G.; Gallucci, E.; and Scrivener, K., "Influence of Limestone on the Hydration of Portland Cements," *Cement and Concrete Research*, V. 38, No. 6, 2008, pp. 848-860. doi: 10.1016/j.cemconres.2008.01.002

60. Lothenbach, B.; Winnefeld, F.; Alder, C.; Wieland, E.; and Lunk, P., "Effect of Temperature on the Pore Solution, Microstructure and Hydration Products of Portland Cement Pastes," *Cement and Concrete Research*, V. 37, No. 4, 2007, pp. 483-491. doi: 10.1016/j.cemconres.2006.11.016

61. Jelitto, H., and Schneider, G. A., "A Geometric Model for the Fracture Toughness of Porous Materials," *Acta Materialia*, V. 151, 2018, pp. 443-453. doi: 10.1016/j.actamat.2018.03.018

62. Jelitto, H., and Schneider, G. A., "Fracture Toughness of Porous Materials–Experimental Methods and Data," *Data in Brief*, V. 23, 2019, Article No. 103709. doi: 10.1016/j.dib.2019.103709

63. Kulik, D. A.; Wagner, T.; Dmytrieva, S. V.; Kosakowski, G.; Hingerl, F. F.; Chudnenko, K. V.; and Berner, U. R., "GEM-Selektor Geochemical Modeling Package: Revised Algorithm and GEMS3K Numerical Kernel for Coupled Simulation Codes," *Computational Geosciences*, V. 17, No. 1, 2013, pp. 1-24.

64. Deschner, F.; Lothenbach, B.; Winnefeld, F.; and Neubauer, J., "Effect of Temperature on the Hydration of Portland Cement Blended With Siliceous Fly Ash," *Cement and Concrete Research*, V. 52, 2013, pp. 169-181. doi: 10.1016/j.cemconres.2013.07.006

65. Kulik, D. A., "Improving the Structural Consistency of C-S-H Solid Solution Thermodynamic Models," *Cement and Concrete Research*, V. 41, No. 5, 2011, pp. 477-495. doi: 10.1016/j.cemconres.2011.01.012

66. Glosser, D.; Suraneni, P.; Isgor, O. B.; and Weiss, W. J., "Estimating Reaction Kinetics of Cementitious Pastes Containing Fly Ash," *Cement and Concrete Composites*, V. 112, 2020, Article No. 103655. doi: 10.1016/j.cemconcomp.2020.103655

67. Taylor, H. F. W., *Cement Chemistry*, Thomas Telford, London, UK, 1997, 459 pp.

68. Powers, T. C., and Brownyard, T. L., "Studies of the Physical Properties of Hardened Portland Cement Paste," *ACI Journal Proceedings*, V. 43, No. 9, Nov. 1946, pp. 249-336.

69. Chandler, H. W.; Merchant, I. J.; Henderson, R. J.; and Macphee, D. E., "Enhanced Crack-Bridging by Unbonded Inclusions in a Brittle Matrix," *Journal of the European Ceramic Society*, V. 22, No. 1, 2002, pp. 129-134. doi: 10.1016/S0955-2219(01)00242-4

70. Liu, D.; Šavija, B.; Smith, G. E.; Flewitt, P. E. J.; Lowe, T.; and Schlangen, E., "Towards Understanding the Influence of Porosity on Mechanical and Fracture Behaviour of Quasi-Brittle Materials: Experiments and Modelling," *International Journal of Fracture*, V. 205, No. 1, 2017, pp. 57-72. doi: 10.1007/s10704-017-0181-7

71. Birchall, J. D.; Howard, A. J.; and Kendall, K., "Flexural Strength and Porosity Of Cements," *Nature*, V. 289, No. 5796, 1981, pp. 388-390. doi: 10.1038/289388a0

72. Dugdale, D. S., "Yielding of Steel Sheets Containing Slits," *Journal of the Mechanics and Physics of Solids*, V. 8, No. 2, 1960, pp. 100-104. doi: 10.1016/0022-5096(60)90013-2

73. Barenblatt, G. I., "The Mathematical Theory of Equilibrium Cracks in Brittle Fracture," *Advances in Applied Mechanics*, V. 7, 1962, pp. 55-129. doi: 10.1016/S0065-2156(08)70121-2

74. Hillerborg, A.; Modéer, M.; and Petersson, P.-E., "Analysis of Crack Formation and Crack Growth in Concrete by Means of Fracture Mechanics and Finite Elements," *Cement and Concrete Research*, V. 6, No. 6, 1976, pp. 773-781. doi: 10.1016/0008-8846(76)90007-7

75. Hibbit, H. D.; Karlsson, B.; and Sorensen, E., "Abaqus Analysis User's Manual," Version 6.12, Simulia, Providence, RI, 2012.

76. ASTM C305-20, "Standard Practice for Mechanical Mixing of Hydraulic Cement Pastes and Mortars of Plastic Consistency," ASTM International, West Conshohocken, PA, 2020, 3 pp.

77. Fu, T., and Weiss, W. J., "The Ball-On-Three-Ball (B3B) Test–Application to Cement Paste and Mortar," *Advances in Civil Engineering Materials*, V. 9, No. 1, 2020, pp. 128-142. doi: 10.1520/ACEM20180070

78. Swamy, R. N., "Dynamic Poisson's Ratio of Portland Cement Paste, Mortar and Concrete," *Cement and Concrete Research*, V. 1, No. 5, 1971, pp. 559-583. doi: 10.1016/0008-8846(71)90060-3

79. Börger, A.; Supancic, P.; and Danzer, R., "The Ball on Three Balls Test for Strength Testing of Brittle Discs: Stress Distribution in the Disc," *Journal of the European Ceramic Society*, V. 22, No. 9-10, 2002, pp. 1425-1436. doi: 10.1016/S0955-2219(01)00458-7

80. Erbektas, A. R.; Isgor, O. B.; and Weiss, J. W., "Comparison of Chemical and Biogenic Acid Attack on Concrete," *ACI Materials Journal*, V. 117, No. 1, Jan. 2020, pp. 255-264. doi: 10.14359/51720293

81. Fu, T.; Montes, F.; Suraneni, P.; Youngblood, J.; and Weiss, J., "The Influence of Cellulose Nanocrystals on the Hydration and Flexural Strength of Portland Cement Pastes," *Polymers*, V. 9, No. 9, 2017, Article No. 424. doi: 10.3390/polym9090424

82. Qiao, C.; Suraneni, P.; and Weiss, J., "Flexural Strength Reduction of Cement Pastes Exposed to CaCl$_2$ Solutions," *Cement and Concrete Composites*, V. 86, 2018, pp. 297-305. doi: 10.1016/j.cemconcomp.2017.11.021

83. ASTM C78/C78M-21, "Standard Test Method for Flexural Strength of Concrete (Using Simple Beam With Third-Point Loading)," ASTM International, West Conshohocken, PA, 2021, 5 pp.

84. Sant, G.; Bentz, D.; and Weiss, J., "Capillary Porosity Depercolation in Cement-Based Materials: Measurement Techniques and Factors Which Influence Their Interpretation," *Cement and Concrete Research*, V. 41, No. 8, 2011, pp. 854-864. doi: 10.1016/j.cemconres.2011.04.006

85. Bentz, D. P., and Garboczi, E. J., "A Digitized Simulation Model for Microstructural Development," *Ceramic Transactions*, V. 16, 1990, pp. 211-226.

86. Bentz, D. P., and Garboczi, E. J., "Percolation of Phases in a Three-Dimensional Cement Paste Microstructural Model," *Cement and Concrete Research*, V. 21, No. 2-3, 1991, pp. 325-344. doi: 10.1016/0008-8846(91)90014-9

87. Trifone, L., "A Study of the Correlation Between Static and Dynamic Modulus of Elasticity on Different Concrete Mixes," MS thesis, West Virginia University, Morgantown, WV, 2017, 105 pp.

88. Wang, B.; Han, Y.; and Liu, S., "Effect of Highly Dispersed Carbon Nanotubes on the Flexural Toughness of Cement-Based Composites," *Construction and Building Materials*, V. 46, 2013, pp. 8-12. doi: 10.1016/j.conbuildmat.2013.04.014

89. Lange, D. A.; Jennings, H. M.; and Shah, S. P., "The Influence of Pore Structure on the Properties of Cement Paste: Initial Observations about Research-In-Progress," *MRS Online Proceedings Library*, V. 137, 1988, pp. 47-54.

90. Nguyen, V. P.; Stroeven, M.; and Sluys, L. J., "Multiscale Continuous and Discontinuous Modeling of Heterogeneous Materials: A Review on Recent Developments," *Journal of Multiscale Modelling*, V. 03, No. 04, 2011, pp. 229-270. doi: 10.1142/S1756973711000509

91. Rim, J. E.; Zavattieri, P.; Juster, A.; and Espinosa, H. D., "Dimensional Analysis and Parametric Studies For Designing Artificial Nacre," *Journal of the Mechanical Behavior of Biomedical Materials*, V. 4, No. 2, 2011, pp. 190-211. doi: 10.1016/j.jmbbm.2010.11.006

92. Espinosa, H. D., and Zavattieri, P. D., "A Grain Level Model for the Study of Failure Initiation and Evolution in Polycrystalline Brittle Materials. Part I: Theory and Numerical Implementation," *Mechanics of Materials*, V. 35, No. 3-6, 2003, pp. 333-364. doi: 10.1016/S0167-6636(02)00285-5

93. Espinosa, H. D., and Zavattieri, P. D., "A Grain Level Model for the Study of Failure Initiation and Evolution in Polycrystalline Brittle Materials. Part II: Numerical Examples," *Mechanics of Materials*, V. 35, No. 3-6, 2003, pp. 365-394. doi: 10.1016/S0167-6636(02)00287-9

94. Qudoos, A.; Atta-ur-Rehman; Kim, H. G.; and Ryou, J.-S., "Influence of the Surface Roughness of Crushed Natural Aggregates on the Microhardness of the Interfacial Transition Zone of Concrete With Mineral Admixtures and Polymer Latex," *Construction and Building Materials*, V. 168, 2018, pp. 946-957. doi: 10.1016/j.conbuildmat.2018.02.205

95. Xiao, J.; Li, W.; Sun, Z.; Lange, D. A.; and Shah, S. P., "Properties of Interfacial Transition Zones in Recycled Aggregate Concrete Tested by Nanoindentation," *Cement and Concrete Composites*, V. 37, 2013, pp. 276-292. doi: 10.1016/j.cemconcomp.2013.01.006

96. Zimbelmann, R., "A Contribution to the Problem of Cement-Aggregate Bond," *Cement and Concrete Research*, V. 15, No. 5, 1985, pp. 801-808. doi: 10.1016/0008-8846(85)90146-2

97. Husem, M., "The Effects of Bond Strengths between Lightweight and Ordinary Aggregate-Mortar, Aggregate-Cement Paste on the Mechanical Properties of Concrete," *Materials Science and Engineering: A*, V. 363, No. 1-2, 2003, pp. 152-158. doi: 10.1016/S0921-5093(03)00595-1

98. Weiss, J.; Couch, J.; Pease, B.; Laugesen, P.; and Geiker, M., "Influence of Mechanically Induced Cracking on Chloride Ingress in Concrete," *Journal of Materials in Civil Engineering*, ASCE, V. 29, No. 9, 2017, p. 04017128. doi: 10.1061/(ASCE)MT.1943-5533.0001922

99. Chen, X.; Wu, S.; and Zhou, J., "Influence of Porosity on Compressive and Tensile Strength of Cement Mortar," *Construction and Building Materials*, V. 40, 2013, pp. 869-874. doi: 10.1016/j.conbuildmat.2012.11.072

100. Zhang, H.; Gan, Y.; Xu, Y.; Zhang, S.; Schlangen, E.; and Šavija, B., "Experimentally Informed Fracture Modelling of Interfacial Transition Zone at Micro-Scale," *Cement and Concrete Composites*, V. 104, 2019, Article No. 103383. doi: 10.1016/j.cemconcomp.2019.103383

101. Konsta-Gdoutos, M. S.; Batis, G.; Danoglidis, P. A.; Zacharopoulou, A. K.; Zacharopoulou, E. K.; Falara, M. G.; and Shah, S. P., "Effect of CNT and CNF Loading and Count on the Corrosion Resistance, Conductivity and Mechanical Properties of Nanomodified OPC Mortars," *Construction and Building Materials*, V. 147, 2017, pp. 48-57. doi: 10.1016/j.conbuildmat.2017.04.112

102. Al-Rifaie, W. N.; Mahdi, O. M.; and Ahmed, W. K., "Development of Nanocement Mortar as a Construction Material," *Advanced Materials Research*, V. 795, 2013, pp. 684-691. doi: 10.4028/www.scientific.net/AMR.795.684

103. Kumar, R., and Bhattacharjee, B., "Porosity, Pore Size Distribution and In Situ Strength of Concrete," *Cement and Concrete Research*, V. 33, No. 1, 2003, pp. 155-164. doi: 10.1016/S0008-8846(02)00942-0

104. Mondal, P.; Shah, S. P; and Marks, L. D., "Nanomechanical Properties of Interfacial Transition Zone in Concrete," *Nanotechnology in Construction 3: Proceedings of the NICOM3*, Z. Bittnar, P. J. M. Bartos, J. Němeček, V. Šmilauer, and J. Zeman, eds., Springer, Berlin, Germany, 2009, pp. 315-320. doi: 10.1007/978-3-642-00980-8_42

105. Jebli, M.; Jamin, F.; Malachanne, E.; Garcia-Diaz, E.; and El Youssoufi, M. S., "Experimental Characterization of Mechanical Properties of the Cement-Aggregate Interface in Concrete," *Construction and Building Materials*, V. 161, 2018, pp. 16-25. doi: 10.1016/j.conbuildmat.2017.11.100

106. Esmaeeli, H. S.; Shishehbor, M.; Weiss, W. J.; and Zavattieri, P. D., "A Two-Step Multiscale Model to Predict Early Age Strength Development of Cementitious Composites Considering Competing Fracture Mechanisms," *Construction and Building Materials*, V. 208, 2019, pp. 577-600. doi: 10.1016/j.conbuildmat.2019.02.134

107. Santos, A. R.; do Rosário Veiga, M.; Silva, A. S.; and de Brito, J., "Microstructure as a Critical Factor of Cement Mortars' Behaviour: The Effect of Aggregates' Properties," *Cement and Concrete Composites*, V. 111, 2020, Article No. 103628. doi: 10.1016/j.cemconcomp.2020.103628

APPENDIX A

In this section, we carry out an RVE size analysis to determine the smallest RVE needed for the simulations. We consider three mortar beams (with dimensions of 25 x 25 x 125 mm^3) with square RVEs of l_r=15mm, l_r = 20mm and l_r = 24 mm, which are analyzed under 3PB condition with the same material properties. To avoid boundary effects, the highest RVE is defined as 1mm away from the top of the beam. In each case, we vary the shape and spatial distribution of aggregates , while keeping the aggregate volume fraction constant. Figure A-1 shows the f'_{tm} predictions for the three RVE sizes. The f'_{tm} predicted by the beams with RVE sizes of l_r = 15mm, 20mm and 24mm is 9.56±0.34Mpa, 8.33±0.32Mpa and 8.49±0.18Mpa, respectively. These comparisons confirm that the f'_{tm} predictions of samples with l_r =20mm and l_r =24mm are very close given the error bars. As such an RVE size of l_r = 20mm is selected for the rest of the simulations.
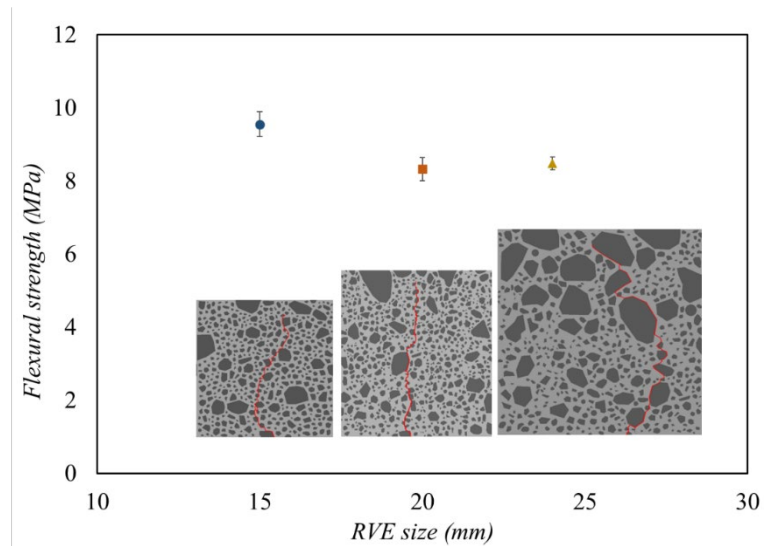
Figure A-1. Flexural strength prediction for mortar beams containing RVE sizes of
l_r=15mm, l_r = 20mm and l_r = 24 mm

APPENDIX B

The purpose of this study is to evaluate the effect of the aggregate volume fraction (f_{agg}) on the f'_{tm} prediction. For such task, we consider mortar beams (with dimensions of 25 x 25 x 125 mm^3) with RVEs that have a statistically representative f_{agg} of 28.6%, 34.3%, and 40.3%, which are analyzed under 3PB condition with the same material properties. In addition, in our meso-mechanical model, we consider that sand particles smaller than a few hundred microns are covered by hydration products and do not behave as aggregates, so they are excluded from the RVEs.[108,109] In the experiment described in section 3.4, the f_{agg} of the mortar beam is 50%, and roughly 20% of the sand particles are smaller than 300 microns (are excluded from the RVEs). Thus, we estimate the maximum f_{agg} in our model to be around 40%. Figure 12 illustrates the f'_{tm} predictions as a function of f_{agg}. The peak stress obtained with RVE with f_{agg} of 28.6%, 34.3%, 40.3% is 11.97 MPa, 12.26 MPa, and 12.30MPa, respectively. We can see the f'_{tm} predictions are close to each other and the average f'_{tm} prediction from three RVEs is 12.18±0.18MPa. From the 3PB experiment described in section 3.4, the error bar of the f'_{tm} is 0.53 MPa. The results show that the error bar of f'_{tm} numerical prediction is small when compared to experiments, indicating that the different f_{agg} only cause a minor amount of variation for f'_{tm} numerical prediction, and the effect of the f_{agg} on the f'_{tm} prediction can be ignored.
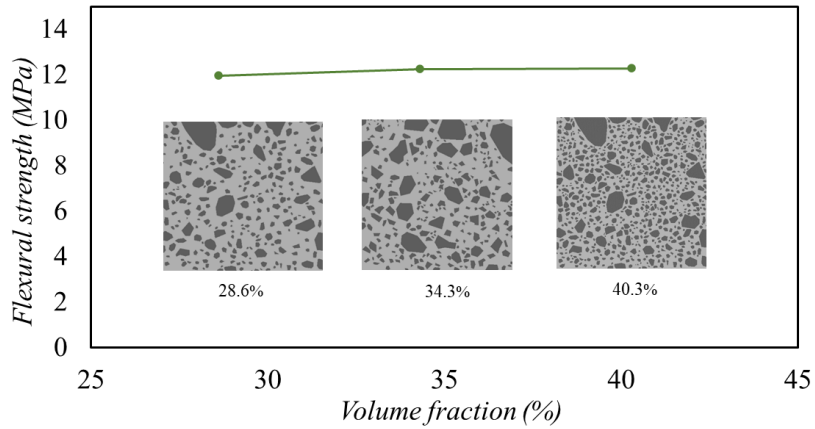
Figure B-1. Flexural strength predictions for RVEs with aggregate volume fraction of 28.6%, 34.3%, and 40.3%

REFERENCES

108. Ergün, A., "Effects of the Usage of Diatomite and Waste Marble Powder as Partial Replacement of Cement on the Mechanical Properties of Concrete," *Construction and Building Materials*, V. 25, No. 2, 2011, pp. 806-812. doi: 10.1016/j.conbuildmat.2010.07.002

109. Cyr, M.; Lawrence, P.; and Ringot, E., "Mineral Admixtures in Mortars: Quantification of the Physical Effects of Inert Materials on Short-Term Hydration," *Cement and Concrete Research*, V. 35, No. 4, 2005, pp. 719-730.